

COMPARATIVE EVALUATION OF HYPERSPECTRAL ANOMALY DETECTION METHODS IN SCENES WITH DIVERSE COMPLEXITY

OECD CONFERENCE CENTER, PARIS, FRANCE / 8–10 FEBRUARY 2012

D. Borghys⁽¹⁾, I. Kasen⁽²⁾, V. Achard⁽³⁾, C. Perneel⁽¹⁾

⁽¹⁾ Royal Military Academy, Av. de la Renaissance 30, Brussels, Belgium, Email: Dirk.Borghys@rma.ac.be

⁽²⁾ Norwegian Defence Research Establishment (FFI), Kjeller, Norway, Email: Ingebjorg.Kasen@ffi.no

⁽³⁾ French Aerospace Laboratory (ONERA), Toulouse, France, Email: Veronique.Achard@onera.fr

KEYWORDS: hyperspectral data, anomaly detection, security, image processing

ABSTRACT:

Anomaly detection in hyperspectral data has received a lot of attention for various applications and is especially important for defence and security. The aim of anomaly detection is to detect pixels in the hyperspectral data cube whose spectra differ significantly from the background spectra.

Many types of anomaly detectors have been proposed in literature. They differ by the way the background spectra are defined and described and by the method used for determining the difference between the pixel under test and the estimated background characteristics.

The most well-known anomaly detector is the RX detector. Several detectors have been derived from the basic RX detector.

On the other hand methods based on image segmentation have also been introduced. These are particularly useful in areas characterised by a highly structured background (e.g. urban scenes).

The current paper presents a comparison of the results obtained by representative examples of two classes of anomaly detector: the RX-family of detectors and the segmentation-based detectors.

1. INTRODUCTION

Many types of anomaly detectors (ADs) have been proposed in literature [1]. The most frequently used anomaly detector is the Reed-Xiaoli (RX) detector [2]. Different variations of this method have been proposed in literature [3, 4, 5, 6, 7]. On the other hand, and mainly for complex scenes (urban and industrial scenes), segmentation-based anomaly detectors (SBAD) have also been introduced [7, 10, 11]. The current paper compares the results of a selected number of examples of both AD classes

when applied to hyperspectral datacubes of different complexity. In particular two rural scenes with sub-pixel anomalies, a rural scene with some targets in shadow and an urban scene were considered.

2. ANOMALY DETECTION METHODS

2.1 RX-based methods

The RX detector [2] is a standard in anomaly detection. Basically the RX detector calculates the Mahalanobis distance between the pixel under test (PUT) and the background:

$$D_{RX} = (r - \mu_B)^T C_B^{-1} (r - \mu_B)$$

C_B and μ_B are respectively the sample spectral covariance matrix and the spectral mean of the background pixels; r is the spectrum of the PUT.

Many different implementations of the RX detector have been proposed in literature. They differ in the way the background covariance matrix and background mean is defined and estimated. In the current paper different types of global RX methods as well as local RX and quasi-local RX are applied.

Global RX (GRX)

The GRX detector estimates the covariance matrix and mean of the background using all pixels of the image. GRX therefore has no parameters. GRX is applied after dimension reduction based on a Kurtosis criterion.

Complementary Subspace Detector (CSD)

In the CSD the highest variance principal components (PCs) are used to define the background subspace and the others (the complementary subspace) the target subspace [4]. The PUT is then projected on the two subspaces and the anomaly detector is the difference of the projection onto the target subspace and the background subspace. Spectral whitening is

applied as pre-processing step.

Sub-space RX (SSRX)

In this paper SSRX is the GRX applied after PCA and the background statistics are determined on a limited number of PCA bands. Usually the first PCs are discarded in SSRX.

RX after orthogonal subspace projection (OSPRX)

In OSPRX the background is defined by the first components of a Singular Value Decomposition. These first components define the background subspace and the data are projected onto the orthogonal subspace before applying the RX detector [1].

Partialling Out RX detector (PORX)

In this method the effect of the clutter in a pixel is partialled out component-wise by predicting each of its spectral components as a linear combination of its high-variance principal components [5]. The detector applies a Mahalanobis distance on the residual.

CSD, SSRX, OSPRX and PORX have only one parameter: the number of spectral bands considered to belong to the background.

Local RX (LRX)

In this case the covariance matrix and mean is determined locally in a window around the PUT. A double sliding window is used: A guard window and an outer window are defined and the background statistics are determined using the pixels between the two. The covariance matrix is regularized using diagonal loading before inversion [8]. The scale factor for the diagonal loading used here is the median of the eigenvalues of the covariance matrix calculated on the complete image. Parameters of LRX are the guard and outer window sizes (GWS, OWS). LRX is applied after dimension reduction based on a Kurtosis criterion.

Quasi-local RX (QLRX)

In quasi-local RX the global covariance matrix is decomposed using eigenvector/eigenvalue decomposition [6]: $C_B = U\Lambda U^T$. The eigenvectors are kept in the RX, but the eigenvalues are replaced by the maximum of the local variance and the global eigenvalue. This means that the score of the detector will be lower at locations of the image with high variance (e.g. edges) than in more homogeneous areas. Spectral statistical standardization is applied as a pre-processing step. The local variance is determined in a double sliding window. Parameters are OWS and GWS.

2.2 Segmentation-based methods

Class-Conditional RX (CCRX)

Although CRX is also an RX-based method, it is cataloged here under Segmentation-Based Anomaly Detectors (SBADs) because it is also based on image segmentation.

In CRX the image is first segmented, the covariance matrix and mean within each class is determined. The Mahalanobis distance between the PUT and each of the classes is calculated. The final result is the minimum of these distances. In the current paper K-means clustering is used and the parameters of the method are minimum number of pixels allowed in each classes and the maximum number of classes used in the clustering. NC, the number of classes, follows on these parameters

The CRX is applied after dimension reduction based on a Kurtosis criterion.

Method based on Multi-normal mixture models (MMM)

A Stochastic Expectation Maximization (SEM) algorithm [9] is used for fitting a multi-normal mixture to the image for describing the background. The anomaly detector detects pixels having a low probability according to the estimated model. The MMM was applied after spectral binning [14] and square root transformation of the data in order to make the noise signal independent [13]. The parameters of the method are the number of mixture components and the termination threshold for the iterative parameter estimation method.

Two-level endmember selection method (TLES)

The principle of this method [10] is the following: a small scanning window (50x50 pixels) runs over the image and at each position of the window the principal background spectra are determined using a segmentation method based on end-member selection. Endmembers that correspond to a minimum percentage (MP) of the image tile are stored.

At the end of the process an endmember selection is again applied on the stored endmembers and linear unmixing is applied on the image. Anomalies correspond to pixels with a large residue after unmixing. The parameters of the method are the number of endmembers in the first and last stage and MP. In [10] N-FINDR was used as the endmember selection method. In the current paper the minimum volume simplex analysis algorithm (MVSA) [11] was used because it was found to give better results.

Method based on a Self-Organizing Map (SOM)

A trained SOM is considered as a representation of

the background classes in the scene. Anomalies are determined by computing the spectral distances of the pixels from the SOM units [12]. The SOM was applied on the first PCA components and run using a square map consisting of $N_s \times N_s$ hexagonal cells. It was optimized sequentially and its parameters are N_s and the number of PCA bands used.

3. IMAGE DATABASE

The analysis was performed on a set of 4 hypercubes of scenes with varying complexity and representative of three scenarios:

- sub-pixel detection in a rural environment
- detection in a rural environment with some of the targets in shadow
- detection of anomalies in an urban environment

Fig. 1 shows an RGB composite for the two datasets with sub-pixel anomalies. In Fig. 2 the dataset with targets in shadow and the urban dataset are shown. The locations of the different targets are also indicated. Tab. 1 presents the main characteristics of the dataset used in the paper. The first column is the name by which the scenes will be referred to further in this paper.



Figure 1: RGB composites of datacubes of CAM and OSL1



Figure 2: RGB color composites of BJO and OSL2 with target locations indicated.

Name	Site	Sensor name	# bands	Waveband μm	Image Size	# tgts	#tgt pixels	Scene description	Type of anomalies
CAM	Camargue(Fr)	HyMap	118	0,41-2,45	150x100	45	45	Agricultural area	green paint
OSL1	Oslo(No)	HySpex	80	0.41-0.98	286x287	81	81	Park near Oslo	green fabric
BJO	Bjoerkelangen (No)	HySpex	80	0.41-0.98	700x1600	14	574	Forest and fields	different materials
OSL2	Oslo(No)	HySpex	80	0.41-0.98	700x1600	4	45	City center of Oslo	green fabric, blue plastic

Table 1: Overview of image database

In the datasets CAM and OSL1 a matrix of anomalies was inserted artificially. Fig. 1 shows these images with full-pixel anomalies. The results shown in this paper were obtained in images with 10% mixing ratio sub-pixel anomalies for the CAM scene. For OSL1 the mixing ratio was varied from 100% down to 10%.

In the BJO scene 14 targets of different sizes and materials are present. Tab. 2 presents the size of the different targets in pixels. Targets 3-7 are in shadow. Figure 2 (left) shows a RGB composite of the BJO scene. A cyan colored rectangle delimits the bounding boxes of each target. Target 3 is hidden in the trees, the 4 other targets in shadow are located at the edge of the forest.

T1	T2	T3	T4	T5	T6	T7
8x22	5x11	4x3	2x3	5x7	4x4	3x3
T8	T9	T10	T11	T12	T13	T14
2x7	3x4	8x10	5x7	4x7	5x8	7x16

Table 2: Target sizes (in pixels) in the BJO scene

In OSL2 four targets are present (see figure 2 right) with respective sizes 5x10 5x9 2x6 6x7 pixels. Two of them consist of green fabric and the other two of a blue plastic. The first three were laid out on the grass in a park, the fourth was laid on an asphalt background.

The images BJO, OSL1 and OSL2 were not georectified before processing and all processing was applied to radiance data, i.e. without applying atmospheric correction.

4. IMPLEMENTATION ISSUES AND EVALUATION METHODOLOGY

5. Pre-processing

Before applying the actual anomaly detectors, some pre-processing methods were applied to the data. The pre-processing technique used depends on the dataset and on the anomaly detector.

Spectral whitening

The RX-based methods were applied with and without spectral whitening and the best result obtained is reported in this paper (see results section). For CSD spectral whitening is always applied. If the eigenvalues and eigenvectors of the covariance matrix of the complete image are resp. Λ and U and μ is the average spectral vector of the image, then the spectral whitening of the pixel r is given by: $r^W = U\Lambda^{-1}U^T(r - \mu)$

Whether whitening is beneficial for the anomaly detector depends on the AD method and the datacube.

Shadow detection

In the case of images that exhibit large contrast between shadow and sunny parts, a classification step in two classes shadow/sunny can be inserted prior to the selection of spectral features and AD. It relies on the fact that radiance in NIR bands is very low in shadow, because there is no direct irradiance and the Rayleigh scattering effects that decrease with the wavelength power 4, induce low diffuse irradiance, too. Then, the histogram of NIR radiances of the image exhibits a first mode for low values that corresponds to shadow parts of the image. (fig. 3 and fig. 4).

This shadow/sunny classification has been applied prior to GRX and CRX for the BJO and OSL2 image. In the CRX method the shadow class counts as an additional class.

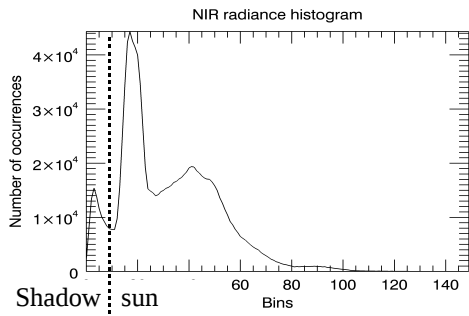


Figure 3: Histogram of NIR radiances of BJO image



Figure 4: BJO shadow mask

6. Evaluation methodology

Experimental ROC (Receiver Operating Characteristics) curves, showing the detection rate (DR) vs. the false alarm rate (FAR), are used to evaluate the results obtained with the various

detectors. For the images with resolved targets, a pixel based ROC curve is calculated for each target, whereas for the images with subpixel targets, a ROC curve is calculated based on all the targets in the image. DR is plotted vs. the *logarithm* of the FAR (the resulting curve is referred to as a logROC), and the area under the logROC curve (the logAUC) is calculated and used as the measure of performance. The reason for using a logarithmic FAR scale is that it ensures equal weight across the range of FAR values.

7. RESULTS AND DISCUSSION

8. Results for CAM and OSL1

Tab. 3 presents the logAUC results obtained for CAM10. It can be seen that LRX, CRX and MMM give the best results. Of the global RX-based methods OPSRX gives the best results.

Fig. 5 shows the logAUC for the OSL1 scene for the different detectors versus the mixing ratio. In this experiment the mixing ratio was varied from 100% (full pixel anomaly) to 10%. Results of global RX-based methods are shown as solid lines, the LRX and QLRX as dot-dash lines and the segmentation-based methods as dashed lines. CRX and LRX clearly give the overall best results. The next best results are obtained by MMM. From the global RX-based methods the OPSRX and SSRX give the best results.

GRX	SSRX	PORX	OSPRX	CSD	LRX
0.732	0.743	0.569	0.931	0.868	1
QLRX	CRX	TLES	SOM	MMM	
0.72	1	0.129	0.116	1	

Table 3: logAUC for CAM10

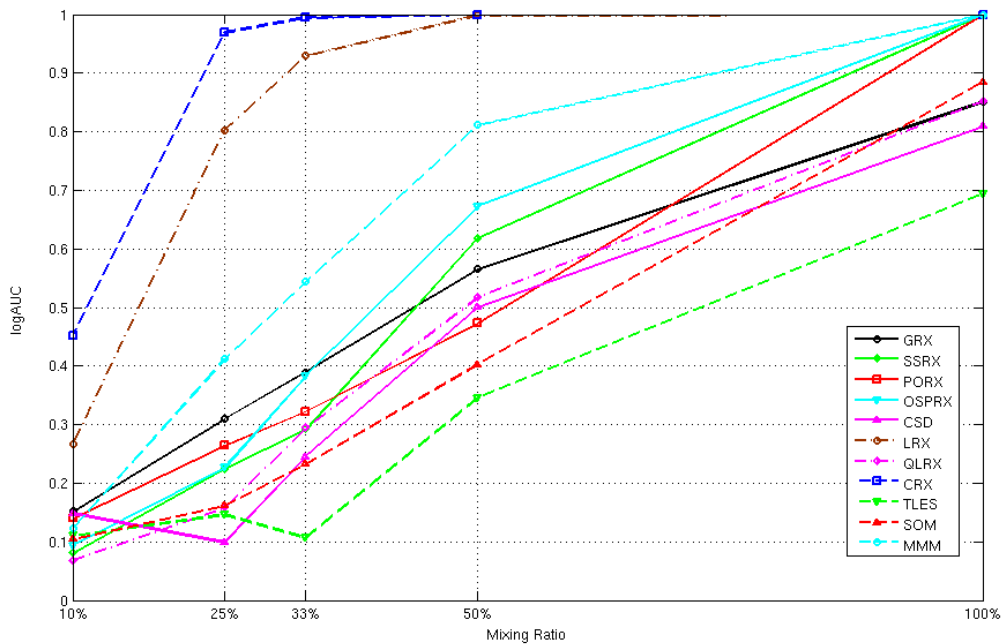


Figure 5: Results of logAUC vs. mixing ratio for OSL1 and for the different detectors

While the MMM gives very good results, the three other segmentation-based methods give quite bad results. Even at full-pixel target size CSD, QLRX, TLES and SOM fail to achieve a unity logAUC.

9. Results for BJO

In the BJO scene 14 targets are present (see fig 2), labelled T1 to T14. Targets T3-T7 are in shadow areas.

Figure 6 shows a graphical representation of the logAUC for each of the detectors and for each target. The colours represent the value of the logAUC. From the figure it is immediately clear that

T2 is the most easily detectable target. It is also clear that the targets in shadow are more difficult to detect than the others. Target 3, hidden in the forest, is the most difficult to detect. For the targets in shadow MMM gives the overall best results, followed by GRX and CRX, both after shadow masking, and LRX. None of the other global RX-based methods give good results. For the targets that are not in shadow areas the MMM and CRX give the globally best results, applying the shadow mask to the GRX and CRX degrades the results, except for T1. MMM gives the most consistent results over all targets.

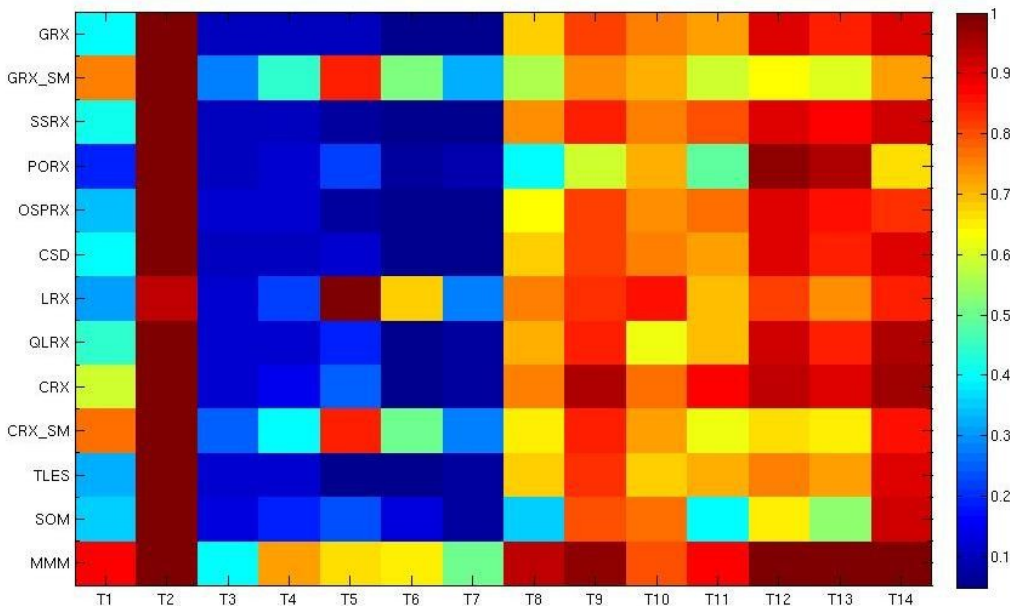


Figure 6: logAUC values for all detectors and each target for the BJO scene.

10. Results for OSL2

Figure 7 shows the logAUC results for the OSL2 scene. It can be seen that the values of logAUC are much lower than for the other data cubes. The maximum value obtained here is 0.54. This is due to the complexity of the scene: the targets inserted into the scene are not the only anomalies. In an urban environment many objects can present an anomalous spectrum, e.g. cars, special roof materials, etc. The comparison therefore only shows how well the different anomaly detection methods cope with this urban “clutter”.

From fig. 7 it can be seen that MMM gives the overall best results, followed by TLES, LRX and SOM. From the global RX methods, OSPRX gives the best results. The shadow mask presents a benefit for T4, which is the only target in shadow. For this target GRX_SM gives the best results. Figure 8 shows the ROC curves obtained by the best detector (MMM) for the four targets in the OSL2 scene. The figure shows that 80% of the target surface is detected at a false alarm rate between 10^{-3} and 10^{-2} .

The first detection for the different targets is reached between a false alarm rate of 10^{-4} and 10^{-3} . Fig. 9 shows the detection image of the MMM detector. It can be seen that the “false alarms” are mainly cars and structures on the roofs of buildings.

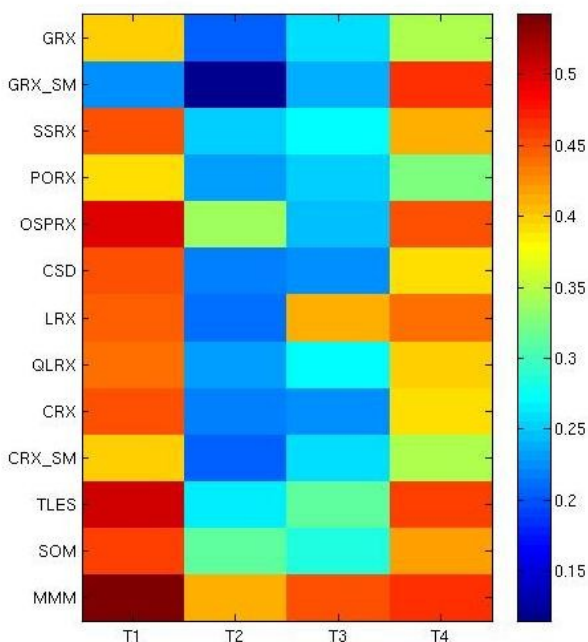


Figure 7: logAUC results for OSL2

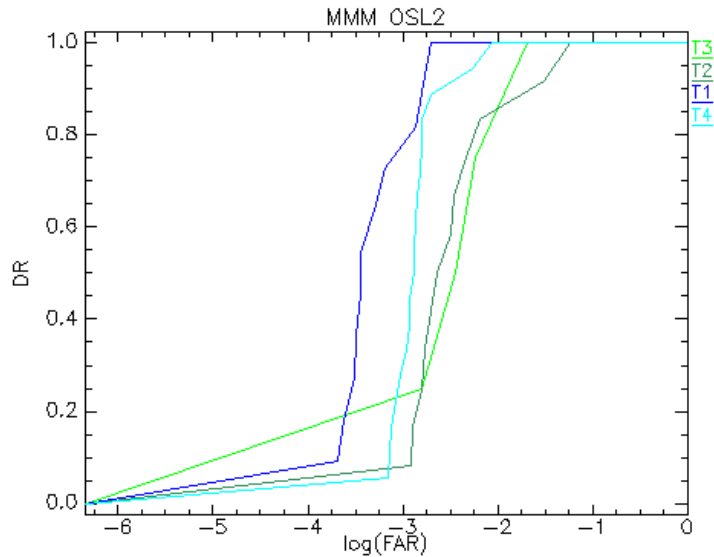


Figure 8: ROC curves obtained by MMM for the four targets in OSL2.

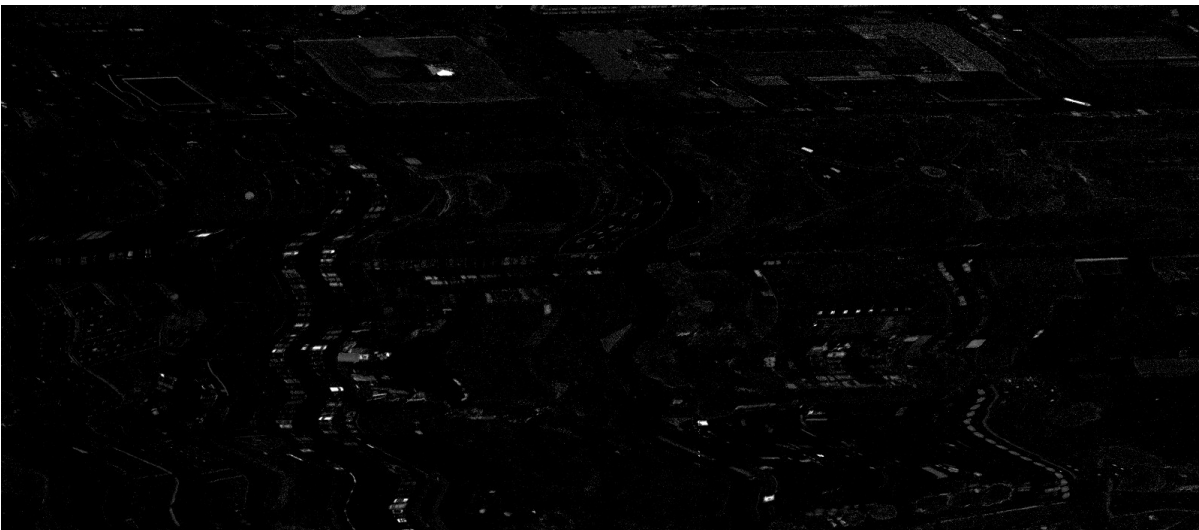


Figure 9: MMM detection images for OSL2

11. CONCLUSIONS

This paper evaluates the performance of anomaly detection methods in scenes with diverse complexity. RX-based and segmentation-based AD methods were applied to four dataset, representing a rural environment with sub-pixel targets, a rural environment with part of the targets in shadow and an urban environment.

For sub-pixel anomaly detection, LRX gives the best results, followed by MMM. From the investigated global RX-based methods OSPRX gives the best results.

For the rural scene with part of the targets in shadow, MMM gives the best overall results. The targets in shadow are also well detected by GRX

and CRX after applying shadow mask. The shadow mask however degrades performance of these two detectors for targets that are not in shadow. This phenomenon will be investigated in further work.

In the urban environment the SBAD methods give generally better results than the RX-based methods. Of the global RX-based methods, OSPRX gives the best results. The overall best result for the urban scene is obtained by MMM.

The influence of pre-processing on the results was very evident. Further work will examine this further.

12. ACKNOWLEDGEMENTS

The authors would like to acknowledge Salvatore

Resta at the University of Pisa for providing the ground truth for the OSL2 data set.

The OSL1, OSL2 and BJO datasets were provided by the Norwegian Defence Research Establishment (FFI). The CAM scene was provided by ESA (DAISEX experiment) through a collaboration with ONERA.

13. REFERENCES

1. S. Matteoli, M. Diani, and G. Corsini, "A tutorial overview of anomaly detection in hyperspectral imagery," *IEEE A&S Systems Magazine, Part3: Tutorials*, vol. 21, no. 3, June 2010.
2. I.S. Reed and X. Yu, "Adaptive multiband cfar detection of an optical pattern with unknown spectral distribution," *IEEE ASSP*, vol. 38, no. 10, pp. 1760–1770, Oct 1990.
3. D.W.J. Stein, S.G. Beaven, L.E. Hoff, E.M. Winter, A.P. Schaum, and A.D. Stocker, "Anomaly detection from hyperspectral imagery," *IEEE Signal Proc. Mag.*, vol. 38, pp. 58–69, Jan 2002.
4. A. Schaum, "Hyperspectral anomaly detection: Beyond RX," in *Proc. SPIE Algorithms and Technologies for Multispectral, Hyperspectral and Ultraspectral Imagery XII*, 2007, vol. 6565.
5. E. Lo and A. Schaum, "A hyperspectral anomaly detector based on partialling out a clutter subspace," in *Proc. SPIE Algorithms and Technologies for Multispectral, Hyperspectral and Ultraspectral Imagery XV*, 2009, vol. 7334.
6. C.E. Caefer, J. Silverman, O. Orthal, D. Antonelli, Y. Sharoni, and S.R. Rotman, "Improved covariance matrices for point target detection in hyperspectral data," *Optical Engineering*, vol. 47, no. 7, July 2008.
7. H. Kwon and N.M. Nasrabadi, "Kernel rx-algorithm: A nonlinear anomaly detector for hyperspectral imagery," *IEEE-TGRS*, vol. 43, no. 2, pp. 388–397, Feb 2005.
8. S. Matteoli, M. Diani, and G. Corsini, "Different approaches for improved covariance matrix estimation in hyperspectral anomaly detection," in *Proc. Annual Meeting Italian National Telecommunications and Information Theory Group - GTTI*, 2009.
9. P. Masson and W. Pieczynski, "SEM algorithm and unsupervised segmentation of satellite images," *IEEE-TGRS*, vol. 31, no. 3, pp. 618–633, Mar 1993.
10. D. Borghys, E. Truyen, M. Shimoni, and C. Perneel, "Anomaly detection in hyperspectral images of complex scenes," in *Proc. 29th Earsel Symposium*, Chania, June 2009.
11. J. Li and J.M. Biucas-Dias, "Minimum Volume Simplex Analysis: a fast algorithm to unmix hyperspectral data", *Proc. IGARSS* 2008.
12. O. Duran and M. Petrou, "Spectral unmixing with negative and superunity abundances for subpixel anomaly detection," *IEEE-GRSL*, vol. 6, no. 1, pp. 152–156, Jan 2009.
13. T. Skauli, "Sensor noise informed representation of hyperspectral data, with benefits for image storage and processing", *Optics Express*, Vol. 19, No. 14, 2011.
14. I. Kåsen, A. Rødningsby, T. V. Haavardsholm, T. Skauli, "Band selection for hyperspectral target detection based on a multinormal mixture anomaly detection algorithm", *Proc. SPIE* 6966, 2008.